Results in Chemistry 16 (2025) 102419

Contents lists available at ScienceDirect

Results in Chemistry

journal homepage: www.sciencedirect.com/journal/results-in-chemistry

Raman spectroscopy for determination of compositions in liquid–liquid dispersions

Alexandra Weber-Bernard, Jörn Viell *

RWTH Aachen University, Aachener Verfahrenstechnik – Process Systems Engineering, Forckenbeckstraße 51, 52074 Aachen, Germany

ARTICLE INFO

Keywords:
Raman spectroscopy
Indirect hard modeling
Binary liquid mixture
Liquid–liquid dispersion
2-methyltetrahydrofuran
Multiplicative light scattering
Molecular association

ABSTRACT

Raman spectroscopy is widely applied for monitoring compositions of chemicals in liquid systems. However, its applications to liquid–liquid dispersions, especially regarding the full composition range, remain limited. Feasibility is in question due to the inherent heterogeneity and the resulting light scattering effects of dispersions. To address this problem, we analyze a uniformly mixed binary liquid mixture of 2-methyltetrahydrofuran and water in both homogeneous phases and their disperse state. We identify effects of heterogeneity on Raman spectra and minimize their impact on quantification through pretreatment. Three alternative quantification methods are compared: peak integration, indirect hard modeling, and partial least-squares regression. For indirect hard modeling, impact of model flexibility on the model fit of the standard two-component model is discussed. Motivated by molecular association observed during spectra analysis, an alternative model with a third component for hydrates of 2-methyltetrahydrofuran is developed. Our results indicate that the accuracy of the models is similar for the aqueous phase and disperse state. Best predictions for these two regions are achieved by indirect hard modeling with three components, which additionally gives reliable predictions of compositions in the organic phase. These insights enable further research on the application of Raman spectroscopy in liquid–liquid dispersions.

1. Introduction

Liquid–liquid dispersions have been utilized in a wide range of processes, including emulsion polymerization or multi-phase reactions. They are relevant to several industries, e.g., food, pharmaceuticals, and chemicals [1]. The Organocat process developed by Grande et al. [2] is an example for a process using a liquid–liquid dispersion. Its aim to separate lignocellulose into its components is achieved by means of vigorous mixing in a biphasic liquid system of 2-methyltetrahydofuran (2-MTHF) and water, with the intention of maximizing the contact area between phases [3,4]. Such large contact areas as well as the simple downstream processing via decantation are the mayor advantages of liquid–liquid dispersions. Despite their advantages, dispersions exhibit complex behavior that still require intensive experimental investigations [5–7]. They occur as oil-in-water or as water-in-oil dispersions depending on various preconditions, such as volume fraction, phase chemical composition, or droplet size (distribution) [1,8]. Modifying these parameters, i.e., changing composition by addition of the solvent, may trigger (catastrophic) phase inversion [9], which happens within a few seconds [10], and changes the dispersed into the continuous phase and vice versa. Secondary dispersions with droplets of the continuous phase inside of the dispersed phase may occur [11–13]. As observed by Liu et al. [10], especially the oil-in-water-in-oil type of secondary dispersions occurs.

Inline spectroscopy, either Raman or Infrared (IR) spectroscopy, is a promising tool for investigating concentrations and has been successfully applied for quantification in aerosols [14] and slurries [15,16]. However, its applications to liquid–liquid dispersions, especially regarding the full composition range, are limited. Compared to IR spectroscopy, Raman spectroscopy is better suited for application liquid–liquid dispersions with an aq phase because of its low sensitivity towards water. Raman spectroscopy allows a quantitative evaluation of the compositions within processes. As such, it enables a target-oriented process optimization [17]. However, liquid–liquid dispersions are rarely explored by Raman spectroscopy, despite their potential, because droplets influence Raman spectra in the form of multiplicative light scattering. Their sizes, shapes, packing and surface [18,19] result in changes to the optical pathways and alter spectral expression of chemical compounds. Both intensity and baseline of Raman spectra are affected [20] by these light scattering effects. This effect can also be visually observed in liquid–liquid dispersions as turbidity. These physicochemical effects can be mitigated using immersion probes with

* Correspondence to: Forckenbeckstraße 51, 52074 Aachen, Germany.
E-mail address: joern.viell@avt.rwth-aachen.de (J. Viell).

https://doi.org/10.1016/j.rechem.2025.102419
Received 21 February 2025; Accepted 2 June 2025
Available online 30 June 2025

Nomenclature

Abbreviations

2-MTHF	2-Methyltetrahydrofuran
2-MTHF(aq)	2-MTHF with hydrogen bonds
2-MTHF(org)	pure 2-MTHF without hydrogen bonds
2c	Two-component model
2c-med	Two-component model with medium interaction
2c-min	Two-component model with minimum interaction
3c	Three-component model
3c-min	Three-component model with minimum interaction
aq	Aqueous
CHM	Complemental hard modeling
HM	Hard model
IHM	Indirect hard modeling
IR	Infrared
MCR-ALS	Multivariate curve resolution, alternating least squares
med	Medium interaction
min	Minimum interaction
org	Organic
PAT	Process analysis technology
PI	Peak integration
PLS	Partial least-squares
RMSEC	Root mean square error of calibration
RMSECV	Root mean square error of cross-validation
RMSEP	Root mean square error of prediction
SNV	Standard normal variate
THF	Tetrahydrofuran

Symbols

α	Water (2c)
β	2-MTHF (2c)
δ	2-MTHF(org) (3c)
ϵ	2-MTHF(aq) (3c)
γ	Water (3c)
ν	Number of assumed hydrogen bonds for one molecule of 2-MTHF

Subscripts

i	Species for two-component model
j	Phase, either aq or org
k	Species for three-component model

short focal distances to enhance the continuous phase signal. This also reduces the influence of droplets in the focal path. Another workaround is the use of an internal standard [21,22].

Quantification in liquid–liquid dispersions is even more complex since such dispersions are quintessentially binary systems. Binary systems, even quasi-ideal ones, exhibit nonlinearity between Raman intensity and concentration [23,24]. There are three complementary interpretations for this nonlinear relationship: Firstly, nonlinearity may be attributed to concentration units used for calibration. Raman spectra show volume dependence [25]. However, mass fractions are easier to obtain and thus preferred for calibrations of mixtures [26–31]. Van Manen et al. [23] have found that the use of mass-based concentrations is acceptable if the difference of densities between liquids is small. Secondly, molecular association of solvent and solute result in nonlinearity, as they lead to peak deformations and shifts [27,32]. In aqueous systems, peak shifts are attributed to water-solute hydrogen bonding [33–35]. Lastly, any remaining nonlinearity between intensity and concentration in binary systems have been ascribed to micro-heterogeneity [23,24]. While the overall sample seems homogeneous, the content of the focal volume is heterogeneous on a molecular level.

Three main difficulties arise for the application of Raman spectroscopy in liquid–liquid dispersions. Both molecular association and micro-heterogeneity are inherent to binary mixtures, while multiplicative light scattering effects arise from the disperse state. All three make quantification in disperse liquid–liquid systems difficult by inducing nonlinearity between intensity and composition. The objective of this study is therefore to establish Raman spectroscopy for the disperse system of 2-MTHF and water and lay the foundation for quantification of components dissolved in the individual phases. To this end, we analyze Raman spectra of the system's homogeneous and disperse states and identify nonlinearity for the specific system. We reduce the complexity of the system by spectra pretreatment and observe that calibration in disperse systems is less complex than anticipated. Further scattering effects are accounted for in the models to ensure universal applicability as well as to enable future quantification. We compare two standard chemometric methods, peak integration (PI) and partial least-squares (PLS), to indirect hard modeling (IHM). The latter model is examined with respect to model flexibility necessary to cope with nonlinearity of the system. Motivated by molecular association, the number of components is increased from two to three to improve the applicability to partly miscible binary liquid mixtures.

2. Materials and methods

2.1. Experimental

Homogeneous samples. Samples of 2-MTHF (VWR Chemicals, 99 %, stabilized with 150 ppm to 400 ppm BHT) and deionized water (conductivity 0.8 µS cm^{-1}) are prepared in 3 mL glass vials. Spectra are taken with a RXN2 Raman spectrometer (Kaiser Optical Systems, 785 nm, 400 mW) using immersion process probes with a working distance of 3 mm (Kaiser Optical Systems). The choice of the immersion probe allows maximum influence of the dispersed phase as compared to the alternative with a working distance of 0 mm. Cosmic ray filtering and dark subtraction are applied; resolution of each spectrum is 4 cm^{-1}.

Disperse samples. For investigation of the biphasic region, a round bottom flask is filled with 50 mL of 2-MTHF and water (see Fig. A.1). The mixture is stirred with a magnetic stirrer at 1000 rpm to ensure a uniform liquid–liquid dispersion and held at constant temperature via water bath. The Raman immersion probe is inserted a few millimeters into the medium at an angle to avoid air bubbles or droplets to get stuck in the focal volume. Incidence of light is minimized by an opaque sheet. Volume ratio is stepwise adjusted by inducing phase separation. After a waiting period of 5 min to reach equilibrium, a defined volume of the aq phase is replaced with org phase with an 1 ml micro-pipette (training samples), thereby increasing overall 2-MTHF content. For the test samples, the org phase is replaced with aq phase, to reduce 2-MTHF content stepwise. After modification of the composition, mixing is resumed. 10 Raman spectra are taken after a waiting period of 10 min for each step in a spectral range of 160 cm^{-1} to 3290 cm^{-1} with 5 s excitation and 3 accumulations. Evaporation of solvent during the experiment is minimized by sealing the set-up with plugs.

2.2. Modeling

Pretreatment of spectral data. Ten spectra are averaged per composition. All averaged spectra are evaluated from 770 cm^{-1} to 1800 cm^{-1} with PEAXACT Version 5.3. (S-Pact GmbH). The signal of atmospheric O_2 in the immersion probes is excluded in the range from 1545 cm^{-1} to 1565 cm^{-1}. Linear fit subtraction and standard normal variate (SNV) normalization are chosen as pretreatment settings to reduce light scattering effects. Raman spectra are shifted against each other by up to 5 cm^{-1}. The gaseous N_2 at 2329 cm^{-1} is chosen as a reference peak to align spectra and enable further evaluation.

Model calibration. PI, IHM [36] and PLS regression models are calibrated. Ratiometric regression is applied to ensure that the mass balance is met by forcing the sum of all predicted mass fractions to unity [37,38]. In the case of PLS, calibrations are centered and scaled.

Peak integration. One peak range per component is chosen; the water peak from 1575 cm^{-1} to 1716.7 cm^{-1} with straight line baseline; the peak for 2-MTHF from 1400 cm^{-1} to 1560 cm^{-1} with a linear fit baseline. For the disperse region, better results were achieved by shifting the integration range for water to 1670.3 cm^{-1} to 1708.2 cm^{-1}.

Indirect hard modeling. For model creation, pseudo-Voigt profiles are added to the model until improvement of the RMS residuals between model fit and spectrum is negligible ($<10^{-2}$). For the pure component model of water, five pseudo-Voigt profiles are fitted to a pure water spectrum. The pure component model for 2-MTHF(org) is constructed by fitting 21 pseudo-Voigt profiles to a pure 2-MTHF spectrum. Complemental hard modeling (CHM) [39] is applied to obtain the component model for 2-MTHF in the aq phase with 22 pseudo-Voigt profiles. Both a two-component (2c) and a three-component (3c) mixture model were evaluated. Calculations of compositions for calibration of the 3c model are detailed in Appendix D.3.

Partial least-squares. No preparation for PLS calibration is necessary. The rank is chosen as indicated.

Validation of chemometrics. Model performance is assessed by the coefficient of determination R^2, Root Mean Square Error of Calibration (RMSEC), Root Mean Square Error of leave 10 % out Cross-Validation (RMSECV) and Root Mean Square Error of Prediction (RMSEP) [40].

3. Results and discussion

Results and discussion are structured in four parts. In the first section, spectra of 2-MTHF and water mixtures are evaluated in detail for homogeneous and disperse states. Peaks relevant for calibration are assigned and their shift and intensity changes summarized. Nonlinear effects of Raman intensity and baseline are discussed. The second section addresses the preparation of the chemometric models based on the spectra analysis. Choices are made concerning the modeling of the system by PI, IHM and PLS. In the third section, the homogeneous phases are calibrated. The last section deals with the calibration of the disperse region. Both third and last section compare standard chemometric methods PLS and PI to two model versions of IHM. The model that is best suited for quantification in partly miscible binary systems is chosen.

3.1. Evaluation of Raman spectra

Raman spectra in the disperse state of the 2-MTHF and water system in the range of 14 wt% to 96 wt% 2-MTHF are shown in Fig. 1. Regarding the Raman intensity, the disperse range is split into two parts at approx. 45 wt%. Before and after the abrupt drop, an increase in Raman intensity is visible with increasing 2-MTHF composition. Baseline intensities follow this trend (see Fig. C.1). The drop in Raman and baseline intensity at approximately equal volumes coincides with an abrupt decrease in conductivity (see Appendix C.2). This can be interpreted as phase inversion, where Raman intensity and baseline are especially influenced by multiplicative light scattering [21,41,42]. As phase inversion equals a sudden exchange of the continuous and disperse phase, refractive indices, densities, and droplet diameters of the phases invert [41,43]. Accordingly, the refraction of laser light at the boundary phase of each droplet in the dispersion changes instantaneously. Hence, Raman intensity changes continuously with increasing 2-MTHF content but with discontinuity at the point of phase inversion.

The variation and discontinuity of Raman intensity has to be considered when the spectra are evaluated for component compositions. Raman spectra are pretreated with SNV normalization and linear baseline subtraction. For pretreated spectra, Raman intensities before and after phase inversion are comparable and the discontinuity at phase inversion is mitigated substantially. However, even with pretreatment, an artifact in the baseline is observed in the range of 1260 cm^{-1} to 1420 cm^{-1}. Visible as a curvature (see Fig. 3(c)), it might be connected to scattering effects from the glass of the vessel in which the experiment was carried out.

Fig. 2 shows four spectra: pure water, aq phase (13.4 wt% 2-MTHF), org phase (96.5 wt% 2-MTHF) and pure 2-MTHF. Raman intensity of the org phase is higher than that of the aq phase by a factor of ten. This is not visible in Fig. 2 because of SNV normalization but can be surmised from the increased noise in spectra of the aq compared to the org phase. Assignments to 2-MTHF have been made according to Durig et al. [44]. Pure 2-MTHF has a very strong peak at 920.6 cm^{-1} (ring breathing), a strong combined peak at 811.7 cm^{-1} and a very weak peak at 1092.5 cm^{-1} (both ring deformation). A strong intensity peak at 1002.5 cm^{-1} is attributed to ring deformation, α-CH-bending mode (1010 cm^{-1}) as well as stretching and bending of the methyl group (1002.5 cm^{-1} and 982.8 cm^{-1}, respectively). CH_2 and CH_3 deformation peaks are overlapping at 1447.7 cm^{-1}. Pure 2-MTHF shows a very weak peak at 1695 cm^{-1}. The spectrum of pure water consists of five overlapping peaks in the range of 1100 cm^{-1} to 1800 cm^{-1} resulting from OH-bending vibrations. Librational motions of hydrogen-bonded water molecules are partly shown below 1000 cm^{-1} [45].

Nonlinear effects of the binary mixture 2-MTHF and water on Raman spectra are ascribed to molecular association. Only slight changes are observed between pure 2-MTHF and 2-MTHF in the org phase (2-MTHF(org)) in Fig. 2. Differences are almost invisible but present in the form of a very slight (<1 cm^{-1}) peak shift with decreasing content of water. The CH_2 deformation modes (1447.7 cm^{-1} and 1486.6 cm^{-1}) shift up by 0.2 cm^{-1} to higher wavenumbers, while ring deformation modes (810.7 cm^{-1} and 1090.5 cm^{-1}) are shifted by up to 0.6 cm^{-1} to lower wavenumbers. Compared to this, 2-MTHF in the aq phase (2-MTHF(aq)) differs distinctly from pure 2-MTHF. Large parts of the spectrum are shifted to higher wavenumbers by up to 8 cm^{-1}. An example is the ring breathing mode at 921 cm^{-1} which, due to hydrogen bonds forming between the oxygen atom of the ring and the hydrogen atoms of water molecules, leads to a decrease in C–O bond strength, thus implying a decrease in vibration frequency. The change of bonds in the 2-MTHF ring at the same time leads to an adjustment of the ring deformation modes. The weak peak at 1092.5 cm^{-1} shifts to lower wavenumbers by 20 cm^{-1}, similarly to the mode at 811.7 cm^{-1} which is shifted by 10 cm^{-1}. This also results in more distinguished overlapping peaks at 1002.8 cm^{-1}. While the three peaks overlap in the org phase, the ring deformation mode (1015.6 cm^{-1}) and CH_2 rocking mode (990 cm^{-1}) of 2-MTHF(aq) can be separated. Hence, molecular interaction of 2-MTHF differs in org and aq environment and is governed by the hydrogen bonding via the ring oxygen atom [46].

In the disperse region of 2-MTHF and water, Raman spectra recorded from 2-MTHF(aq) to 2-MTHF(org) exhibit very few differences of the features already identified in aqueous or organic state (see Fig. 3). The range from 950 cm^{-1} to 1120 cm^{-1} shows peaks shifts with increasing 2-MTHF content, while Raman intensity increases. Although being weak, both effects are strongly nonlinear (compare intensities

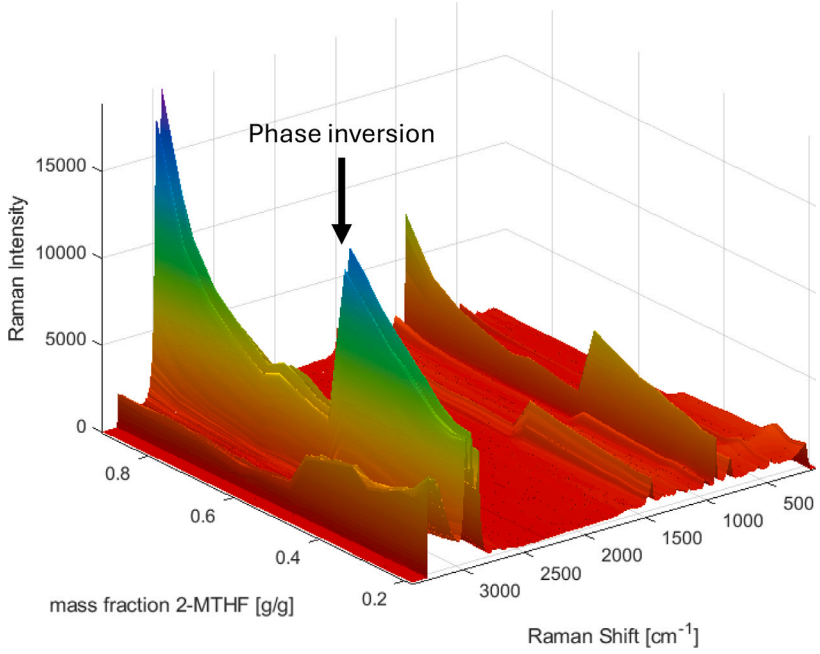

Fig. 1. Variation of Raman intensity over mass fractions in a biphasic 2-MTHF/water mixture at 1400 rpm (see two-dimensional version in Fig. B.1). Stepwise adjustment of mass fractions from aq to org phase. Experiments (Appendix C.2) have shown that phase inversion and the abrupt intensity drop marked by an arrow coincide.

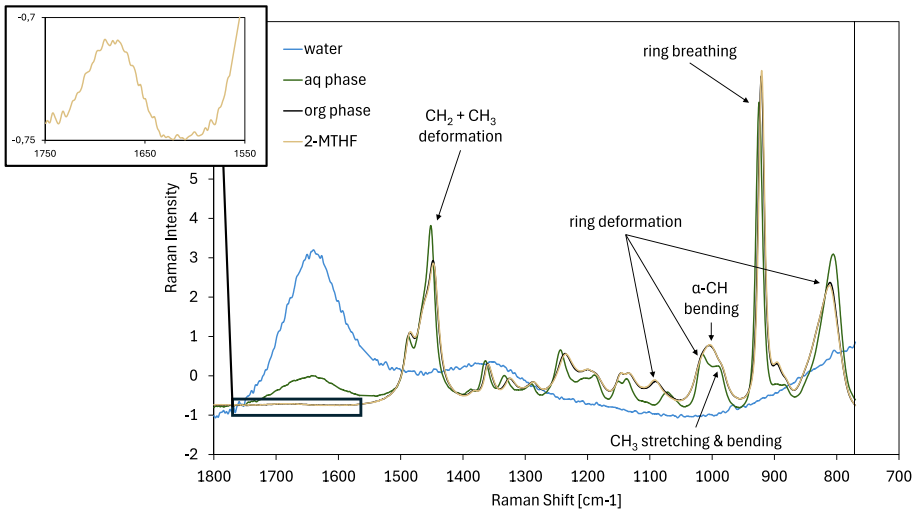

Fig. 2. Raman spectra of 2-MTHF, water, aq and org phase with assignments [44]. Pretreatment: offset subtraction, SNV normalization. Pure 2-MTHF and 2-MTHF in the org phase are almost identical while peaks of 2-MTHF in the aq phase have shifted in position. See peak positions of marked peaks in Table B.1.

in (a) and (b) of Fig. 3; peak area in Fig. D.1) even after spectra pretreatment. Mayerhöfer et al. [24] attribute this nonlinear behavior to micro-heterogeneity.

Hence, the detailed evaluation of Raman spectra in both homogeneous and disperse regions of the 2-MTHF and water system reveal that spectra pretreatment by SNV normalization and a linear baseline allows comparison of spectral features and assignment to molecular groups. They show small but distinct differences allowing to differentiate between molecular states even in the disperse region.

3.2. Preparation of chemometric models

Due to the disperse nature of the system, calibration is carried out for the homogeneous and the disperse state separately. First, three types of models are compared: PI and PLS as representatives of standard chemometric methods and IHM as a physically motivated method. Especially for IHM, the number of components and model flexibility (i.e., the allowed degree of interaction) have to be determined to enable sound comparison.

Univariate modeling is limited to the evaluation of one variable [47] but gives unambiguous evidence of linearity between signal and data. This, however, is subject to the condition that only the component of interest must contribute to the selected peak. For the 2-MTHF and water system, pure 2-MTHF shows a very weak peak at 1695 cm^{-1} that overlaps with the O–H vibrations of water (see enlarged section of Fig. 2). This signal of water would have to be subtracted from the net signal of 2-MTHF to avoid inaccurate predictions of water content in pure 2-MTHF by the PI model. To avoid calibrating outside of the software PEAXACT, the signal was suppressed by careful choice of integration range and baseline.

PLS as a data-driven method is intended for multivariate analysis of overlapping mixture spectra. As a linear method, its limitations concerning nonlinear peak shifts and deformations are known. Although

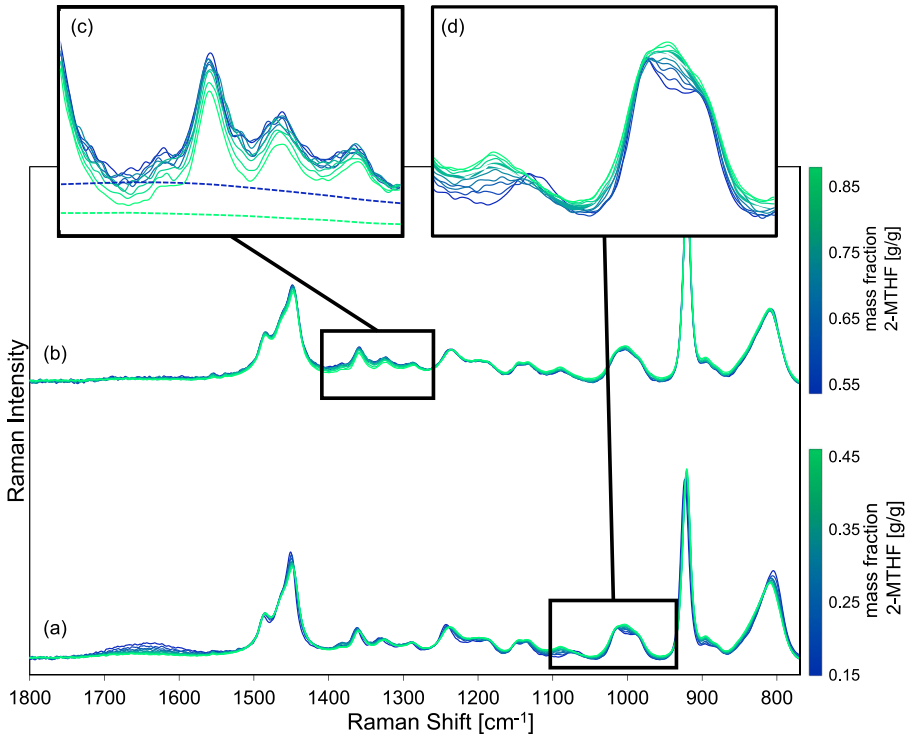

Fig. 3. 2D fingerprint region of the disperse composition range of 2-MTHF and water. Pretreatment: linear subtraction, SNV normalization. (a) Before phase inversion. (b) After phase inversion. Intensity variation before and after phase inversion indicate peak flattening which has been attributed to micro-heterogeneity by Mayerhöfer [24]. (c) Details on nonlinear baseline effects. Dashed lines indicate curvature modeled by pseudo-Voigt profile in IHM. (d) Spectral change from 2-MTHF(aq) to 2-MTHF(org) in the range $950\,\mathrm{cm}^{-1}$ to $1110\,\mathrm{cm}^{-1}$ in detail.

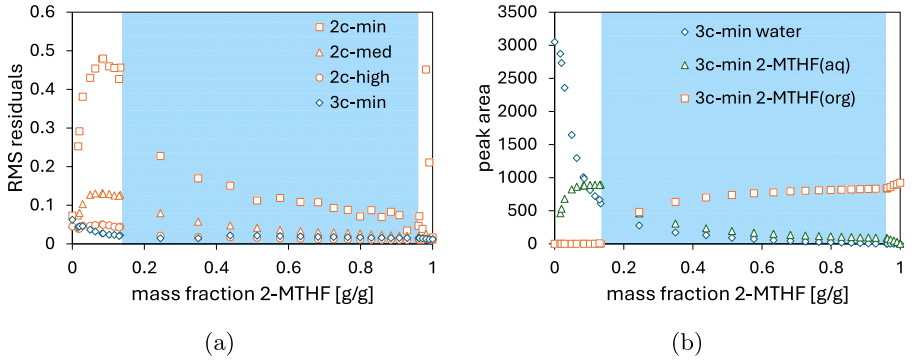

Fig. 4. Component fitting of two-component (2c) and three-component (3c) models to Raman spectra in the 2-MTHF and water system. The blue shaded area indicates the biphasic region. (a) Comparison of RMS residuals of the spectral fit between the model and the measured sample. Residuals of the 2c model with high interaction are in the same order of magnitude as the 3c model with minimum interaction. (b) Peak areas of all components for the 3c version of the mixture model. All three components of water, 2-MTHF(aq), and 2-MTHF(org) exist simultaneously in the heterogeneous disperse region. 2-MTHF(org) is absent in the aq phase, water in the org phase. (For interpretation of the references to color in this figure legend, the reader is referred to the web version of this article.)

large datasets are difficult to obtain in disperse liquid–liquid mixtures, here, PLS is applied to gain an understanding of the disperse system with minimal effort.

IHM has been developed for quantification of overlapping peaks using pseudo-Voigt profiles for each component in a mixture model [36]. The nonlinear influence of multiplicative light scattering can be included as an additional pseudo-Voigt profile, which is not evaluated quantitatively. Major design decisions of IHM are

(i) model flexibility, and
(ii) the number of model components.

Model flexibility – meaning the model's capability of adapting to peak deformations caused by molecular association – is chosen in the form of the so-called fitting mode and encompasses the variation of model parameters from minimum (min) interaction to maximum interaction (see Appendix D.1 for information on fitting modes). We analyze a two-component (2c) model by varying model flexibility in the disperse range with the aim of compensating the differences between 2-MTHF(aq) and 2-MTHF(org). The peak areas resulting from component fitting deviate only slightly between the 2c models, especially peak areas of medium (med) and high interaction are not distinguishable (see Fig. D.1). Analysis of spectral residuals in Fig. 4(a) shows that the model fit is distinctly improved by switching from min to med interaction. High interaction reduces spectral residuals again but no influence on the component fit is discernible (refer to Fig. 4(a)). Therefore, the 2c model with medium interaction (2c-med model) is chosen for the disperse range to balance between spectral features and degree of freedom. Adaption of the model to homogeneous phases by distinguishing between pure component models of 2-MTHF(aq) and

2-MTHF(org) allows further reduction of the degree of freedom. In this case, a 2c-min model for the aq and org phase respectively are combined with a 2c-med model for the disperse phase. This reduces degrees of freedom from 19 to 4 in the homogeneous phases, which decreases computational effort.

An alternative to increasing model flexibility is to increase the number of components in the mixture model. In theory, four components for the modeling of the homogeneous phases of 2-MTHF and water are viable: 2-MTHF in org (2-MTHF(org)) and aq (2-MTHF(aq)) phase and water in both respective phases. While 2-MTHF(org) is equivalent to pure 2-MTHF, 2-MTHF(aq) identifies as a hydrogen-bonded complex of 2-MTHF and water. Water is assumed to exist mainly as bulk water in the aq phase [48] and is mostly bound to 2-MTHF in the org phase [49]. The latter is included in 2-MTHF(aq). Numerical evaluation of the peak areas at $1600\,cm^{-1}$ support this assumption. Although evaluation of the peak areas of the O−H bend signal reveals a small increase in signal strength with water content, it remains negligible.

Compared to the 2c model approach, exploiting molecular association during model building maintains prediction capability at lower computational cost. The approach combines all three pure component models, both 2-MTHF(aq) and 2-MTHF(org) and water to one mixture model. The fit of this mixture model to Raman spectra of all compositions results in Fig. 4(b). Analysis of the component areas shows that 2-MTHF(org) is absent in the aq phase up to 14 wt% of 2-MTHF. This supports the hypothesis that the majority of 2-MTHF molecules present in the aq phase form hydrogen bonds while pure (or self-associated) 2-MTHF is negligible. In addition to hydrogen bonded 2-MTHF(aq), bulk water is present. In the biphasic region, 2-MTHF(org) coexists with bulk water and 2-MTHF(aq). Peak areas of bulk water and 2-MTHF(aq) lie close to each other, which indicates that the impact of 2-MTHF(aq) in the organic phase is low. Finally, in the org phase, the Raman signal from bulk water is negligible and 2-MTHF(aq) and 2-MTHF(org) coexist. This evaluation supports the earlier claim that calibration should be divided into three regions: two homogeneous and one disperse. Fig. 4(a) shows that fit of the three-component model with minimum interaction and component shift (3c-min model) is comparable to high interaction fitting mode for the 2c model. This implies better accuracy at lower computational effort.

While PLS is straightforward in its preparation, PI faces the difficulty of overlapping peaks for the 2-MTHF and water system. For IHM, a decision regarding the number of components and mode of interaction has to be made. It is possible to evaluate a 2c model with medium interaction as well as a 3c model with minimum interaction. These four models were calibrated for the two homogeneous and the disperse region. The results are compared in the following sections.

3.3. Quantification of homogeneous phases

At room temperature, the homogeneous aq phase ranges from 0 wt% to 14 wt% 2-MTHF. The org phase forms from 96 wt% to 100 wt% 2-MTHF. Both phases are calibrated separately and the results compared to each other. Results of calibration and validation are summarized in Table 1 and Fig. 5. PI, IHM and PLS are compared for both aq and org phase individually.

Calibration of the aq phase is straightforward for 2-MTHF and water. PI as well as the 2c-min and 3c-min model of IHM, have RMSEC below 0.25 wt%, similar to results by Glass et al. [50] and Aigner et al. [29]. Validation using a second set shows a slight advantage of PI compared to IHM 2c and 3c models with RMSEP of 0.22 wt% versus 0.34 wt% and 0.35 wt%, respectively. The less complex 2c-min model has a slight advantage compared to the 3c-min model in this case, as the latter has twice the degrees of freedom despite using minimum interaction because of the activated component shift. Compared PI and IHM, results from PLS calibration in the aq phase are distinctly worse. With a rank of three, calibration results are satisfactory at a RMSEC of 0.63 wt%. However, prediction of 2-MTHF content with the validation set shows that the calibrated model cannot predict independent datasets. This reflects the limitations of PLS concerning nonlinear peak shifts and deformations. Hence, apart from PLS, all models show a similarly good fit for both calibration and validation.

Calibration of the org phase is more complicated. Only the 3c-min model is able to achieve acceptable results. As discussed before, little water signal is distinguishable in the org phase of 2-MTHF and water. This is the reason the 2c model fails completely with a negative coefficient of determination and RMSEC of 1.27 wt%. Solubility of water in 2-MTHF being as low as 4 wt%, such errors are considerable. PI performs better with RMSEC of 0.29 wt% but fails validation with an RMSEP of 6.13 wt%. The 3c-min model shows much improvement in that regard. As the majority of water molecules interact with 2-MTHF [49], bulk water becomes negligible. 2-MTHF(aq), as the hydrogen-bonded complex of 2-MTHF and water, is thus proportional to the amount of water in the phase. RMSEC and RMSEP below 0.25 wt% are achieved by calibrating the 2-MTHF(aq) model with the water composition. This is superior to the aq phase and identifies the 3c model as the best option for application to the organic phase. If applicable to other biphasic systems, the use of Raman spectroscopy could be expanded to the whole system. At the moment, a change of alternative analysis method is favored to model the organic phase. For example, Glass et al. [50] apply IR spectroscopy to the organic phase. IR being sensitive to water, they are able to achieve RMSECV of 0.84 wt%. The 3c-min model surpasses these results.

Similar as observed in the aq phase, PLS shows inferior results. While RMSEC of 0.04 wt% is easily achieved with only three ranks, validation fails with RMSEP of 38.98 wt%. The best model for the organic phase is, therefore, the 3c model with minimum interaction.

For calibration of the homogeneous phases, the 3c-min model has been found to be the best choice because of its satisfactory performance in both aq and especially in the org phase. Quality of the 3c model with minimum interaction in the org phase implies the possibility of applying Raman to the complete biphasic system instead of changing to an alternative analysis method.

3.4. Quantification of disperse region

Compared to the homogeneous phases, quantification of the disperse region is more complicated. As a first measure, extrapolation of the homogeneous phase models to the disperse region may seem promising but does not give meaningful results. Predictions deviate distinctly from linearity when outside the model's calibrated range (see Fig. E.1). This underlines the strong nonlinearity of the chosen system. The next simple options is a calibration of the 2c-med model over the whole composition range, from aq phase to org phase (see Fig. E.2). The disadvantage of such a simple model is a large prediction error for the org phase up to 2 wt%. This is unacceptable in context of the low water solubility in 2-MTHF. Therefore, this option is not discussed further. Instead, PI, PLS and IHM models discussed in the section on the preparation of chemometric models are calibrated over the disperse region, including saturated aq and org phase. In the following, this set of spectra will be addressed as the training samples. IHM models comprise both the 2c-med (applied solely to training data from the disperse state) and 3c-min model. Calibrations are validated with another set of spectra in the disperse region, addressed as the test samples. Results for the disperse region are shown in Table 2 as well as visualized in Fig. 5.

The calibration of the 3c-min model comprises 2-MTHF(aq), 2-MTHF(org) and bulk water. The composition of bulk water is corrected with respect to the water molecules in 2-MTHF(aq) (see Appendix D.3). For comparison with the 2c model, predictions of the three components 2-MTHF(aq), 2-MTHF(org) and bulk water are then converted back to the 2-component system of 2-MTHF and water. This is possible by utilizing the predictions of either bulk water or 2-MTHF(org) of the 3c-system. We have chosen 2-MTHF(org) on the basis that the fit of

Table 1
Comparison between PI, IHM and PLS models for aq and org phase. Number of samples and fitting mode for the calibration. Evaluation of predictions for larger datasets and respective other phase.

	aq phase				org phase			
	PI	IHM		PLS	PI	IHM		PLS
		2c-min	3c-min	rank 3		2c-min	3c-min	rank 2
Calibration								
samples	11	11	11	11	4	4	4	4
R^2	0.9963	0.9968	0.9971	0.9770	0.9207	−0.4670	0.9863	0.9985
RMSEC [wt%]	0.25	0.24	0.22	0.63	0.29	1.27	0.12	0.04
RMSECV [wt%]	0.29	0.30	0.28	2.90	0.63	2.03	0.19	0.73
RMSEP								
samples	15	15	15	15	11	11	11	11
aq [wt%]	0.22	0.34	0.35	5.96				
org [wt%]					6.13	2.10	0.25	38.98

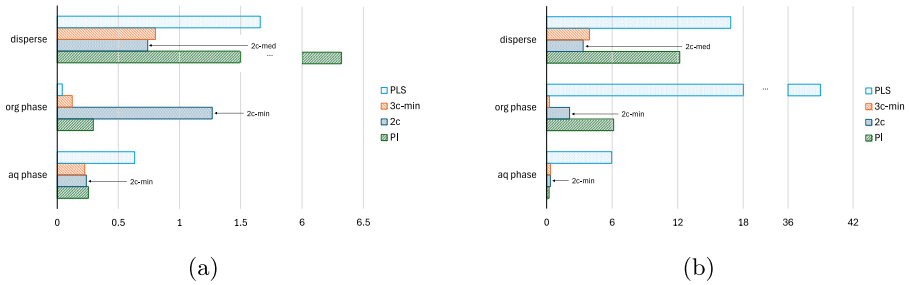

Fig. 5. (a) RMSEC and (b) RMSEP for all models in the homogeneous phases and their dispersion. Arrows indicate either minimum or medium interaction for the two-component (2c) model.

Table 2
Calibration data for PI, IHM and PLS models in disperse region.

	PI	IHM				PLS
		2c-med	3c-min			rank 3
			2-MTHF(aq)	water	2-MTHF(org)	
R^2	0.9323	0.9991	0.9240	0.9982	0.9989	0.9985
RMSEC [wt%]	6.32	0.74	0.51	1.00	0.85	0.04
RMSECV [wt%]	6.59	0.76	0.56	1.07	0.91	0.73
RMSEP [wt%]	12.18	3.34	0.53	4.50	4.13	38.98

the model to the calculated compositions with a RMSEC of 0.85 wt% is better than that of water (RMSEC= 1 wt%). With these restrictions in mind, both 2c-med and 3c-min models achieve comparable results for calibration, with RMSEC of 0.74 and 0.80 wt%, respectively. This may be less exact than most of the results for the homogeneous phases but demonstrates the feasibility of quantification of the disperse phase. Using the 3c-min model equals using one mixture model over the whole composition range. Although three separate calibrations – one per phase and one for the disperse region – are necessary, a clear advantage compared to the 2c model is obvious.

The RMSEP for validation shown in Table 2 are in the same order of magnitude for the 2c-med and 3c-min model. However, with increasing 2-MTHF content, the error of the predictions increases to 6 and 8 wt%, respectively (see Fig. E.3). In contrast to the results, prediction at high 2-MTHF compositions is expected to be particularly good, as measurements are less affected by experimental errors than lower 2-MTHF ratios. Three possible explanations for this behavior exist. Firstly, local temperature effects in the vicinity of the Raman probe are possible. Glass et al. [50] have established that solubility of water in 2-MTHF decreases with increasing temperatures. This would explain the surplus of water that was detected at high 2-MTHF compositions. Secondly, secondary dispersions [10,51] have been observed. With o/w/o secondary dispersions, the ratio of aq to org phase and thus the mass fraction of water of the overall system appears larger than it is as part of the continuous phase is enclosed in the disperse phase. Lastly, incomplete mixing of the biphasic system is possible. Of course, a combination of these three phenomena is possible as well.

Both PI and PLS struggle with predictions in the disperse region. Although the water peak in the PI model was already tuned to achieve the best possible results, both calibration and validation are worse than the other models by a factor of ten. Apparently, with only one peak per component, nonlinearity of the system cannot be sufficiently accounted for. Compared to PI, PLS performs much better, achieving a RMSEC of 1.66 wt%. This is almost on par with the results of IHM. Furthermore, the rank of three that is necessary for these results supports the expansion of IHM to three components. However, an RMSEP of 16.85 wt% for validation indicates that PLS in the disperse region behaves similar to the homogeneous phases. Although a large error in the test set predictions is expected based on observations of the IHM models, the predictions of PLS and IHM are fundamentally different (see Fig. E.3). While deviating at high 2-MTHF composition for IHM, PLS predicts large errors for low compositions of 2-MTHF. Additionally, the phase inversion point is very pronounced in composition prediction despite spectra pretreatment. Consequently, neither PI nor PLS are a viable choice for the disperse region.

Again, the 3c-min model is preferable to the alternative models, as it has less degrees of freedom than the 2c-med model. It uses one mixture model for the whole composition range, although separate calibrations for the homogeneous phases and disperse state are necessary. The

3c-min model gives hints about molecular association in the mixture independent of the entire 2-MTHF and water compositions.

4. Conclusion

We explore the feasibility of quantification using Raman spectroscopy in a liquid–liquid dispersion of 2-MTHF and water, in which experimental parameters such as temperature, geometry, and stirring are kept constant. By modeling the hydrogen-bonded complex of 2-MTHF and water as a separate component, we develop an approach for quantification of the complete binary liquid system. This systematic approach to compare known pure components in both phases with respect to observability can be applied to other biphasic systems. It encompasses the following steps:

(i) systematic analysis of Raman spectra,
(ii) identification of potential pure components, and
(iii) assessment of necessary components based on molecular interaction and spectral data.

For 2-MTHF and water, a three-component mixture model including 2-MTHF(aq), 2-MTHF(org), and water is revealed to be superior and physically justified. An RMSEC of 0.22 wt% and 0.80 wt%, respectively, could be achieved over the whole composition range. In the organic phase, results are exceptionally good with RMSEC values of 0.12 wt%. The extension to other (secondary) liquid–liquid dispersions and fully miscible binary mixtures including the exploration of various states of the system would open various opportunities for Raman spectroscopy in chemistry and process development. Further investigation on the exploitation of multiple light scattering effects to determine dispersion characteristics is of interest.

CRediT authorship contribution statement

Alexandra Weber-Bernard: Writing – original draft, Methodology, Investigation, Formal analysis. **Jörn Viell:** Writing – review & editing, Supervision, Funding acquisition, Conceptualization.

Funding

This research was carried out as a part of the Focus Lab "AP^3 – Advanced pulping for perennial plants: A holistic and sustainable integrated lignocellulose biorefinery concept", a project of the Bioeconomy Science Center (BioSC). The scientific activities of the Bioeconomy Science Center were financially supported by the Ministry of Innovation, Science and Research within the framework of the NRW Strategieprojekt BioSC (no. 313/323-400-002 13).

Declaration of competing interest

The authors declare that they have no known competing financial interests or personal relationships that could have appeared to influence the work reported in this paper.

Acknowledgment

The authors thank Alexander Mitsos for his scientific support and for reviewing and editing. Many thanks to Alexander Echtermeyer, Caroline Marks and Luise Kaven for helpful scientific discussions as well as to Marit Brossmann and Tim Rathaj for their valuable support in performing experiments and Raman spectra acquisition.

Appendix A. Experimental setup

See Fig. A.1.

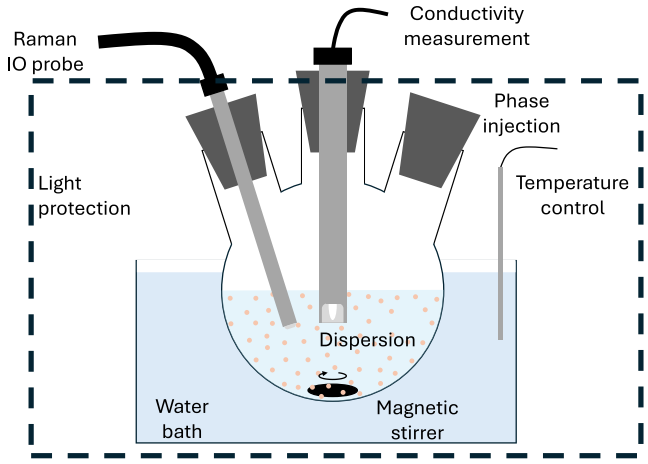

Fig. A.1. Experimental setup in liquid–liquid dispersion monitored by in-line Raman immersion optics (IO) and, in some cases, added by conductivity measurements. Based on Echtermeyer et al. [28].

Table B.1
Peak positions of Raman peaks assigned to 2-MTHF in the aq phase, the org phase, and pure 2-MTHF.

Assignment	2-MTHF [cm^{-1}]		
	aq phase	org phase	pure
CH_2+CH_3 deformation	1451.5	1447.9	1447.7
	1071.7	1090.9	1092.5
ring deformation	1015.6	1019.4[a]	1020.0[a]
	805.3	810.7	811.7
α–CH bending	1002.8[a]	1002.5[a]	1002.5[a]
CH_3 stretching & bending	990.7	983.3[a]	982.8[a]
ring breathing	924.4	920.8	920.6

[a] Peak positions according to fit of pseudo-Voigt profiles to Raman spectrum.

Appendix B. Details on the spectra

B.1. Raman intensities in the disperse range

See Fig. B.1.

B.2. Peak positions in homogeneous phases

See Table B.1.

Appendix C. Details on nonlinear effects

C.1. Effects of disperse system on the baseline

See Figs. C.1 and C.2.

C.2. Confirmation of phase inversion by conductivity measurements

Measurements of conductivity in the disperse region have confirmed that the drop of Raman and baseline intensity is connected to the phenomenon of phase inversion. To this end, the experimental setup in the disperse range that is described in Section 2 is added by 0.1 mg/mL$_{water}$ of NaCl. Conductivity is measured with a standard conductivity measuring cell (WTW TetraCon® 925) that is positioned at similar height in the dispersion as the Raman probe.

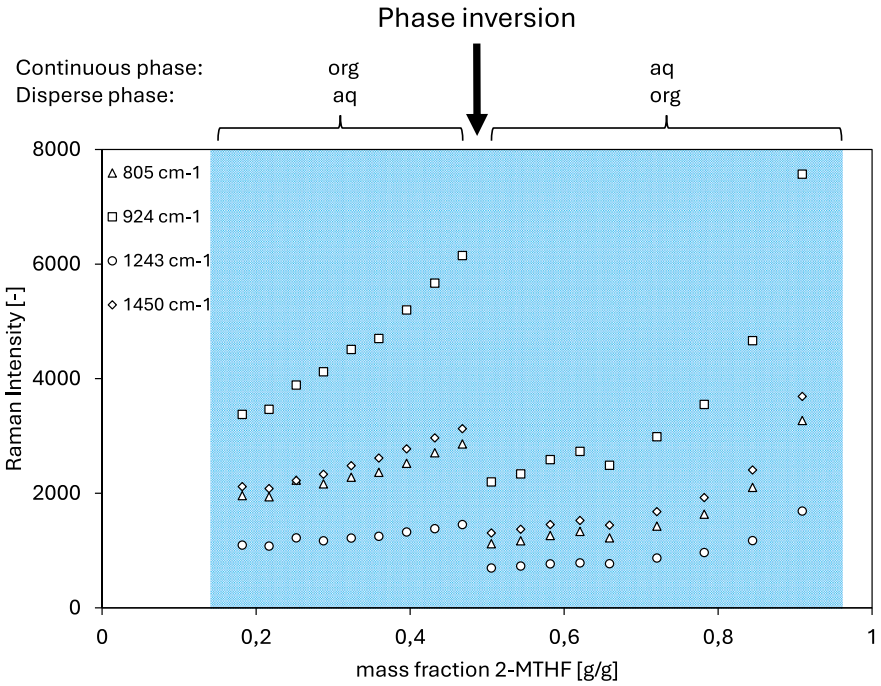

Fig. B.1. 2D-Version of Fig. 1 with Raman intensity over mass fractions for four peaks in the fingerprint region of a disperse 2-MTHF/water mixture at 1400 rpm. Continuous and disperse phase of the regions above and below phase inversion are assigned. The blue shaded area indicates the biphasic region. (For interpretation of the references to color in this figure legend, the reader is referred to the web version of this article.)

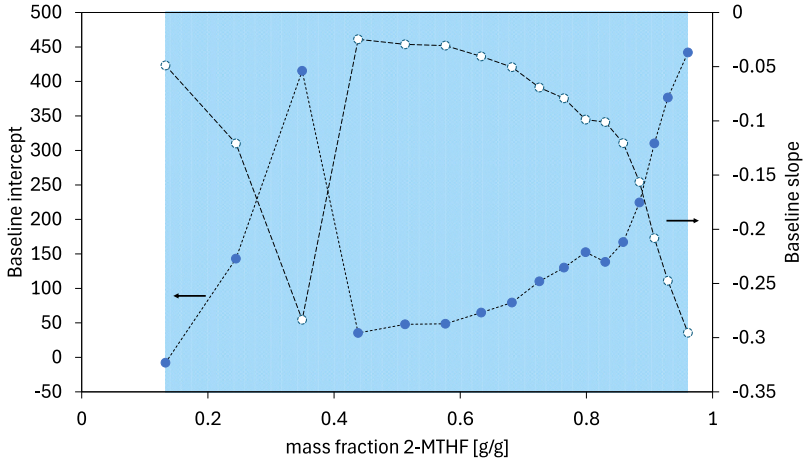

Fig. C.1. Baseline slope and intercept for IHM 2c-med model without pretreatment in the range of 770 cm^{-1} to 1800 cm^{-1}. The blue shaded area indicates the biphasic region. (For interpretation of the references to color in this figure legend, the reader is referred to the web version of this article.)

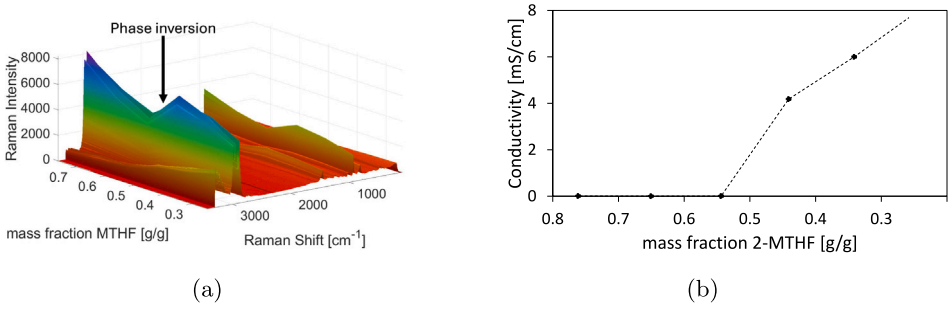

Fig. C.2. Stepwise adjustment of mass fractions of a biphasic 2-MTHF/water mixture with added NaCl at 1400 rpm. (a) Raman spectra without pretreatment. Phase inversion coincides with abrupt intensity drop marked by an arrow. (b) Conductivity measurements where drop in conductivity imply phase inversion at identical mass fraction as with Raman intensity.

Table D.1
Interaction modes and associated degrees of freedom. Component shift is optional.

Interaction mode	Minimum	Medium	High	Maximum	No. of parameters
component shift	(x)	(x)	(x)	(x)	1 per HM
component weights	x	x	x	x	1 per HM
baseline parameters	x	x	x	x	2
peak positions		x	x	x	1 per considered peak
peak parameters			x	x	3 per considered peak

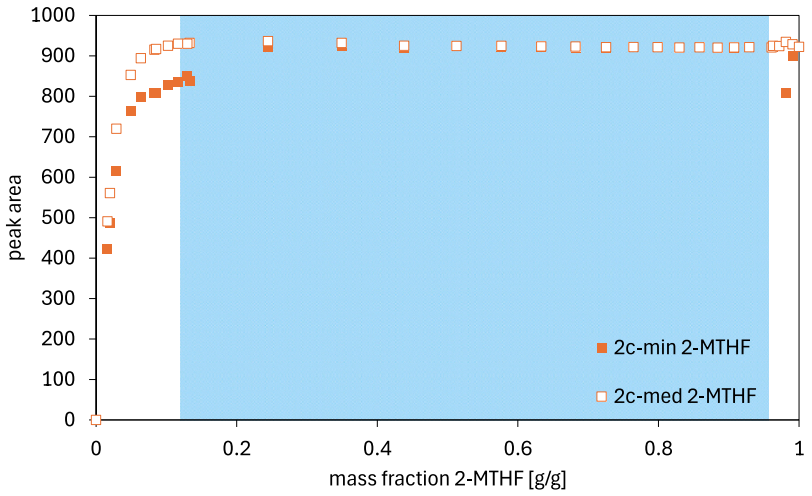

Fig. D.1. Component fitting of the two-component (2c) model. Comparison between minimum interaction (2c-min) and medium interaction (2c-med) for 2-MTHF. The fit of high interaction coincides with 2c-med. The blue shaded area indicates the biphasic region. (For interpretation of the references to color in this figure legend, the reader is referred to the web version of this article.)

Results of the conductivity measurements are shown in Fig. C.2(b). At low 2-MTHF compositions, conductivity is high because of a continuous aq phase. The drop in conductivity around 50 wt% indicates that a change from the continuous aq phase to the continuous org phase has occurred, that is, the phase inversion. At high 2-MTHF compositions, no conductivity is measured which correlates to a continuous org phase. Raman spectra of the experiment (Fig. C.2(a)) show similar behavior to the experiment without NaCl (Fig. 1). Raman intensity increases for low compositions of 2-MTHF and drops at approx. 45 wt%. Afterward, intensity increases again. Thus, it can be concluded that the drop in Raman intensity in Fig. 1 can be assigned to phase inversion. The drop in Raman intensity observed in the system with NaCl being less pronounced than in Fig. 1 is attributed to the influence of NaCl on hydrogen bonding [52].

Appendix D. Details on model building

D.1. Model flexibility for IHM calibration

Four settings for model flexibility are available for IHM in PEAX-ACT [53]. The purpose of this option is to compensate for peak shifts and deformations by increasing the number of adjustable parameters. Each fitting mode, from minimum to high, opens up additional parameters. For high and maximum interaction, the number of peaks considered has to be chosen as computational effort increases drastically with increasing degrees of freedom. Default setting is 15. Only significant peaks, i.e., those that improve the model fit the most, should be adjusted. Component shift is an option that can be selected to shift individual pure component models as a whole. With component shift activated, even minimum interaction mode becomes nonlinear. The increasing degrees of freedom, as shown in Table D.1, include baseline and peak parameters as well as component shift and weights.

D.2. Model flexibility evaluation of two-component model

Component fitting of two-component (2c) model spectra over the 2-MTHF composition range. Significant offset between 2c-min and 2c-med in the aq phase because of peak shifts and deformations due to molecular association. High interaction coincides strongly with medium interaction and is therefore not shown, although residuals (see Fig. 4(a)) reveal slight improvement in fit for high interaction.

D.3. Calculation of compositions for three-component model

Evaluation of Raman spectra from the 2-MTHF ($C_5H_{10}O$) and water system supports the hypothesis that, at the molecular level, the system consists of three components: bulk water, 2-MTHF(aq) and 2-MTHF(org). Analysis of Raman spectra with multivariate curve resolution, alternating least squares (MCR-ALS) in the fingerprint region supports this (not shown). 2-MTHF(aq) is a complex in which 2-MTHF molecule is hydrogen bonded to an unknown number of water molecules. While other complexes (more than one 2-MTHF molecule, different numbers of water molecules) can, in theory, exist, the analysis of the Raman spectra strongly supports one such complex.

$$C_5H_{10}O + \nu H_2O \longrightarrow C_5H_{10}O{-}(H_2O)_\nu$$

Behavior of 2-MTHF is assumed to be similar to tetrahydrofuran (THF) based on the furan ring and additional methyl group. Self-association is assumed to be improbable, as shown in investigations of THF and heavy water [54]. Less than five hydrogen bonds were expected for 2-MTHF(aq) based on investigations on THF by Katayama and Osutsumi [55]. The exact number of hydrogen bonds ν, however, is unknown.

For the homogeneous phases, the overall molar amount of 2-MTHF α and water β is expected to rearrange into bulk water γ, 2-MTHF(org) δ and 2-MTHF(aq) ϵ.

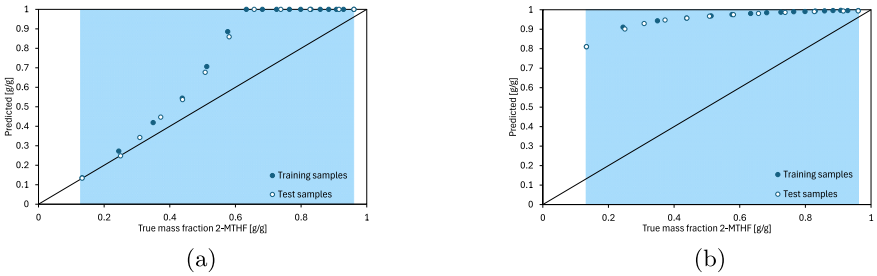

Fig. E.1. Extrapolation of the 2c-min model of the (a) aqueous, and (b) organic phase to the disperse region. The blue shaded area indicates the biphasic region. (For interpretation of the references to color in this figure legend, the reader is referred to the web version of this article.)

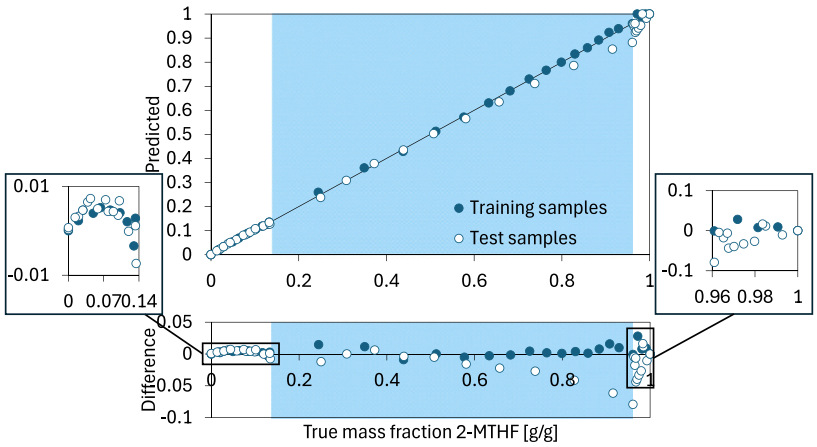

Fig. E.2. Calibration and validation of 2c-med model over the whole composition range. The blue shaded area indicates the biphasic region. (For interpretation of the references to color in this figure legend, the reader is referred to the web version of this article.)

$$n_\alpha H_2O + n_\beta C_5H_{10}O \longleftrightarrow n_\gamma H_2O + n_\delta C_5H_{10}O + n_\epsilon C_5H_{10}O{-}(H_2O)_\nu$$

Component fitting of the 3c-min model (Fig. 4(b)) shows that 2-MTHF(org) δ is negligible in the aq phase, same as water γ is negligible in the org phase. Thus, both homogeneous phases consist of two components only. The amounts of these components in each phase depend on the number of hydrogen bonds ν between 2-MTHF and water. Aq and org phase are shown below, respectively.

$$\text{aq phase:} \quad n_\gamma = n_\alpha - n_\beta\nu \quad \wedge \quad n_\delta = 0 \quad \wedge \quad n_\epsilon = n_\beta$$

$$\text{org phase:} \quad n_\gamma = 0 \quad \wedge \quad n_\delta = n_\beta - \frac{n_\alpha}{\nu} \quad \wedge \quad n_\epsilon = \frac{n_\alpha}{\nu}$$

Mole fractions are calculated both for the original 2c and the additional 3c case and for the aq as well as the org phase.

$$x_{ij} = \frac{n_{ij}}{\sum_i n_{ij}} \quad \forall i = \{\alpha, \beta\} \wedge j = \{\text{aq,org}\} \tag{D.1}$$

$$x_{kj} = \frac{n_{kj}}{\sum_k n_{kj}} \quad \forall k = \{\gamma, \delta, \epsilon\} \wedge j = \{\text{aq,org}\} \tag{D.2}$$

The number of hydrogen bonds ν for 2-MTHF(aq) and 2-MTF(org) are identical based on the assumption of three components for the overall system. Peak areas A for 2-MTHF(org) and 2-MTHF(aq) in the organic phase are used to determine the number of water molecules that bond to 2-MTHF. The aq phase is unsuitable for determination because the amount of bulk water is unknown.

$$\nu = \frac{(\frac{A_{\delta,\text{org}}}{A_{\epsilon,\text{org}}} + 1)x_{\alpha,\text{org}}}{1 - x_{\alpha,\text{org}}} \tag{D.3}$$

With knowledge of the number of hydrogen bonds ν as well as the calibration sample compositions x_α and x_β, all molar fractions of the aq and org phase are calculated by the above defined molar balances. For the disperse region, both the aq and org phase are expected to be present as a dispersion. Molar fractions of the phases have to be transferred to overall compositions. As the nonlinearity of Raman intensity is less pronounced with mass-based composition units, we transfer molar to mass fractions.

$$x_k = \frac{n_k}{\sum_k n_k} \tag{D.4}$$

$$w_k = \frac{m_k}{\sum_k m_k} \tag{D.5}$$

$$M_k = \frac{m_k}{n_k} \tag{D.6}$$

$$M_\epsilon = \nu M_\gamma + M_\delta \tag{D.7}$$

Overall mass fractions are then calculated using the ratios of aq and org phase which are identical to the 2c-system concerning mass fractions.

$$w_{kj} = \sum_j \frac{m_{kj}}{m} = \sum_j w_{kj} w_j \forall k = \{\gamma, \delta, \epsilon\} \wedge j = \{\text{aq,org}\} \tag{D.8}$$

Appendix E. Details on results

This section contains additional details on the presented results. Fig. E.1 confirms that extrapolation of two-component (2c) models to the disperse region is not viable. Fig. E.2 shows calibration over the

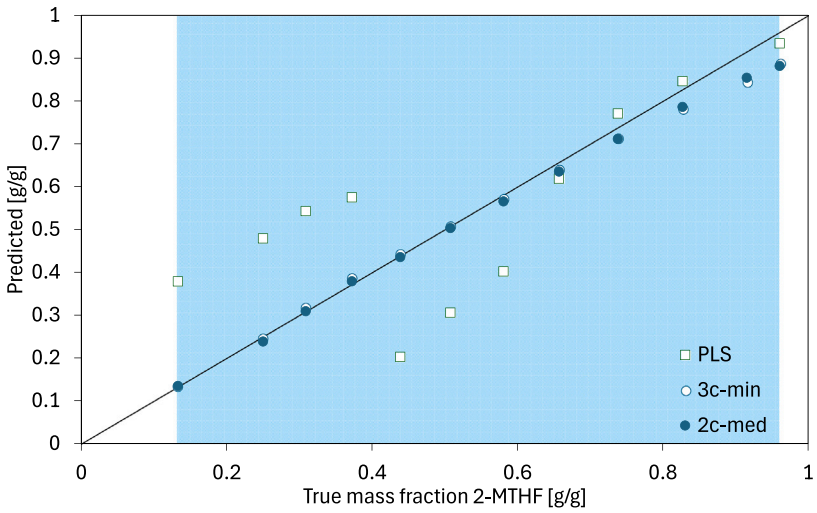

Fig. E.3. Test samples for PLS and IHM models. Offset at high 2-MTHF compositions between true content and model prediction of 6 (2c-med model) or 8 wt% (3c-min model) for IHM, for PLS at low 2-MTHF compositions. The blue shaded area indicates the biphasic region. (For interpretation of the references to color in this figure legend, the reader is referred to the web version of this article.)

complete composition range. Prediction errors of up to 2 wt% for the organic phase are unacceptable regarding low solubility of water in the org phase. Lastly, differences between validation of PLS and IHM model (Fig. E.3) are shown. While the trend of 2c-med and 3c-min models deviates slightly for high 2-MTHF contents, the trend holds. Validation of PLS is in line with the homogeneous phases, prediction errors of up to 24 wt% (at low 2-MTHF content) showing that the model cannot predict independent datasets.

Data availability

Data will be made available on request.

References

[1] M.A. Norato, L.L. Tavlarides, C. Tsouris, Phase inversion studies in liquid–liquid dispersions, Can. J. Chem. Eng. 76 (3) (1998) 486–494.
[2] P.M. Grande, J. Viell, N. Theyssen, W. Marquardt, P.D. de María, W. Leitner, Fractionation of lignocellulosic biomass using the OrganoCat process, Green Chem. 17 (6) (2015) 3533–3539.
[3] D.F. Aycock, Solvent applications of 2-methyltetrahydrofuran in organometallic and biphasic reactions, Org. Process Res. Dev. 11 (1) (2007) 156–159.
[4] V. Pace, P. Hoyos, L. Castoldi, P. Domínguez de María, A.R. Alcántara, 2–Methyltetrahydrofuran (2–MeTHF): A biomass–derived solvent with broad application in organic chemistry, ChemSusChem 5 (8) (2012) 1369–1379.
[5] S. Sibirtsev, C.B. Göbel, A. Jupke, Automation of a procedure for the experimental investigation of liquid–liquid phase separation, Chem. Ing. Tech. 91 (12) (2019) 1787–1793, http://dx.doi.org/10.1002/cite.201900162.
[6] L. Hohl, S. Röhl, M. Kraume, Drop size distributions as a function of dispersed phase viscosity: experiments and modeling, Chem. Eng. Technol. 46 (6) (2023) 1260–1270, http://dx.doi.org/10.1002/ceat.202200589.
[7] G. Kelbaliyev, S. Rasulov, G. Mustafayeva, Viscosity of structured disperse systems, Theor. Found. Chem. Eng. 52 (3) (2018) 404–411, http://dx.doi.org/10.1134/S0040579518020082.
[8] J. Maffi, D. Estenoz, Predicting phase inversion in agitated dispersions with machine learning algorithms, Chem. Eng. Commun. 208 (12) (2021) 1757–1774, http://dx.doi.org/10.1080/00986445.2020.1815715.
[9] M. Rondón-Gonzaléz, V. Sadtler, L. Choplin, J.-L. Salager, Emulsion catastrophic inversion from abnormal to normal morphology. 5. Effect of the water-to-oil ratio and surfactant concentration on the inversion produced by continuous stirring, Ind. Eng. Chem. Res. 45 (9) (2006) 3074–3080, http://dx.doi.org/10.1021/ie060036l.
[10] L. Liu, O.K. Matar, E. Susana Perez de Ortiz, G.F. Hewitt, Experimental investigation of phase inversion in a stirred vessel using LIF, Chem. Eng. Sci. 60 (1) (2005) 85–94, http://dx.doi.org/10.1016/j.ces.2004.07.066.
[11] B. Brooks, H. Richmond, Phase inversion in non-ionic surfactant—oil—water systems—II. Drop size studies in catastrophic inversion with turbulent mixing, Chem. Eng. Sci. 49 (7) (1994) 1065–1075, http://dx.doi.org/10.1016/0009-2509(94)80012-X.
[12] R.D. Vold, Emulsions: theory and practice (Becher, Paul), J. Chem. Educ. 42 (12) (1965) 692.
[13] E. Tyrode, I. Mira, N. Zambrano, L. Márquez, M. Rondón-Gonzalez, J.-L. Salager, Emulsion catastrophic inversion from abnormal to normal morphology. 3. Conditions for triggering the dynamic inversion and application to industrial processes, Ind. Eng. Chem. Res. 42 (19) (2003) 4311–4318, http://dx.doi.org/10.1021/ie0300629.
[14] S. Sinanis, M. Aleksandrova, K. Schaber, Characterization of multicomponent aerosols by raman spectroscopy, Aerosol. Sci. Technol. 45 (6) (2011) 751–757, http://dx.doi.org/10.1080/02786826.2011.559494.
[15] S. XuanYuan, H. Hao, C. Hu, J. Lan, T. Song, C. Xie, Quantitative analysis of solid and liquid contents in reactive crystallization by in-situ Raman with support vector regression, J. Cryst. Growth 587 (2022) 126641, http://dx.doi.org/10.1016/j.jcrysgro.2022.126641.
[16] W. Su, C. Li, H. Hao, J. Whelan, M. Barrett, B. Glennon, Monitoring the liquid phase concentration by raman spectroscopy in a polymorphic system, J. Raman Spectrosc. 46 (11) (2015) 1150–1156, http://dx.doi.org/10.1002/jrs.4745.
[17] B.C. Smith, Quantitative Spectroscopy: Theory and Practice, Academic Press, 2003.
[18] Z.-P. Chen, J. Morris, E. Martin, Extracting chemical information from spectral data with multiplicative light scattering effects by optical path-length estimation and correction, Anal. Chem. 78 (22) (2006) 7674–7681, http://dx.doi.org/10.1021/ac0610255.
[19] H. Martens, E. Stark, Extended multiplicative signal correction and spectral interference subtraction: new preprocessing methods for near infrared spectroscopy, J. Pharm. Biomed. Anal. 9 (8) (1991) 625–635, http://dx.doi.org/10.1016/0731-7085(91)80188-F.
[20] K.H. Lil, E.-O. Rukke, E.F. Olsen, T. Isaksson, Customized baseline correction, Chemom. Intell. Lab. Syst. 109 (1) (2011) 51–56, http://dx.doi.org/10.1016/j.chemolab.2011.07.005.
[21] X. Chen, K. Laughlin, J.R. Sparks, L. Linder, V. Farozic, H. Masser, M. Petr, In situ monitoring of emulsion polymerization by raman spectroscopy: A robust and versatile chemometric analysis method, Org. Process Res. Dev. 19 (8) (2015) 995–1003, http://dx.doi.org/10.1021/acs.oprd.5b00045.
[22] C. Wang, T.J. Vickers, C.K. Mann, Use of water as an internal standard in the direct monitoring of emulsion polymerization by fiber-optic Raman spectroscopy, Appl. Spectrosc. 47 (7) (1993) 928–932.
[23] H.-J. van Manen, J. Gerretzen, M. Smout, G. Postma, J.J. Jansen, Quantitative vibrational spectroscopy on liquid mixtures: concentration units matter, Analyst 146 (10) (2021) 3150–3156, http://dx.doi.org/10.1039/D1AN00151E.
[24] T.G. Mayerhöfer, J. Popp, Beyond Beer's law: spectral mixing rules, Appl. Spectrosc. 74 (10) (2020) 1287–1294, http://dx.doi.org/10.1177/0003702820942273.
[25] H. Mark, J. Workman Jr., Chemometrics in Spectroscopy, Elsevier, 2010.
[26] L.F. Kaven, H.J. Wolff, L. Wille, M. Wessling, A. Mitsos, J. Viell, In-line monitoring of microgel synthesis: flow versus batch reactor, Org. Process Res. Dev. 25 (9) (2021) 2039–2051, http://dx.doi.org/10.1021/acs.oprd.1c00087.
[27] T. Shimoaka, T. Hasegawa, Molecular structural analysis of hydrated ethylene glycol accounting for the antifreeze effect by using infrared attenuated total reflection spectroscopy, J. Mol. Liq. 223 (2016) 621–627, http://dx.doi.org/10.1016/j.molliq.2016.08.097.

[28] A. Echtermeyer, C. Marks, A. Mitsos, J. Viell, Inline raman spectroscopy and indirect hard modeling for concentration monitoring of dissociated acid species, Appl. Spectrosc. 75 (5) (2020) 506–519, http://dx.doi.org/10.1177/0003702820973275.
[29] M. Aigner, A. Echtermeyer, S. Kaminski, J. Viell, K. Leonhard, A. Mitsos, A. Jupke, Ternary system CO2/2-MTHF/Water—Experimental study and thermodynamic modeling, J. Chem. Eng. Data (2019).
[30] R.C. Reid, J.M. Prausnitz, B.E. Poling, The Properties of Gases and Liquids, fourth ed., in: McGraw-Hill Books in Chemical Engineering, McGraw-Hill, New York, 1987.
[31] F. Ebrahimi, J. Viell, A. Mitsos, A. Mhamdi, M. Brandhorst, In-line monitoring of hydrogen peroxide in two–phase reactions using raman spectroscopy, AlChE J. 63 (9) (2017) 3994–4002.
[32] B. Yang, Y. Li, N. Gong, X. Cao, S. Wang, C. Sun, Study of molecular association in acetic acid-water binary solution by Raman spectroscopy, Spectrochim. Acta, Part A 213 (2019) 463–466, http://dx.doi.org/10.1016/j.saa.2018.08.029.
[33] D.T. Bowron, J.L. Finney, A.K. Soper, Structural characteristics of a 0.23 mole fraction aqueous solution of tetrahydrofuran at 20 degrees C, J. Phys. Chem. B. 110 (41) (2006) 20235–20245, http://dx.doi.org/10.1021/jp064170v.
[34] L.C.G. Freitas, J.M.M. Cordeiro, Monte Carlo simulation of water-tetrahydrofuran mixtures, J. Mol. Struct. Theochem 335 (1-3) (1995) 189–195, http://dx.doi.org/10.1016/0166-1280(94)04000-I.
[35] A.Y. Manakov, S.V. Goryainov, A. Kurnosov, A.Y. Likhacheva, Y.A. Dyadin, E.G. Larionov, Clathrate nature of the high-pressure tetrahydrofuran hydrate phase and some new data on the phase diagram of the tetrahydrofuran–water system at pressures up to 3 GPa, J. Phys. Chem. B. 107 (31) (2003) 7861–7866, http://dx.doi.org/10.1021/jp0259925.
[36] F. Alsmeyer, H.-J. Koß, W. Marquardt, Indirect spectral hard modeling for the analysis of reactive and interacting mixtures, Appl. Spectrosc. 58 (8) (2004) 975–985.
[37] J. Meyer-Kirschner, M. Kather, A. Pich, D. Engel, W. Marquardt, J. Viell, A. Mitsos, In-line monitoring of monomer and polymer content during microgel synthesis using precipitation polymerization via raman spectroscopy and indirect hard modeling, Appl. Spectrosc. 70 (3) (2016) 416–426.
[38] J. Meyer-Kirschner, A. Mitsos, J. Viell, Reliable spectroscopic process monitoring using an optimal acquisition time procedure determined by signal-to-noise ratio, Measurement 122 (2018) 100–105.
[39] E. Kriesten, D. Mayer, F. Alsmeyer, C. Minnich, L. Greiner, W. Marquardt, Identification of unknown pure component spectra by indirect hard modeling, Chemom. Intell. Lab. Syst. 93 (2) (2008) 108–119, http://dx.doi.org/10.1016/j.chemolab.2008.05.002.
[40] J.-P. Conzen, Multivariate Kalibration: ein praktischer Leitfaden zur Methodenentwicklung in der quantitaven Analytik, Bruker Optik, 2005.
[41] J. Meyer-Kirschner, A. Mitsos, J. Viell, Polymer particle sizing from raman spectra by regression of hard model parameters, J. Raman Spectrosc. 49 (8) (2018) 1402–1411.
[42] H.-J. van Manen, R. Bloemenkamp, O.F. van den Brink, Focal length determination of raman immersion ball probes in diverse media, Appl. Spectrosc. 63 (3) (2009) 378–380.
[43] L. Yeo, O.K. Matar, E.P. de Ortiz, G.F. Hewitt, Phase inversion and associated phenomena, Multiphase Sci. Technol. 12 (1) (2000) 66, http://dx.doi.org/10.1615/MultScienTechn.v12.i1.20.
[44] J. Durig, K. Kizer, J. Karriker, Spectra and structure of small ring compounds. XXXVI. 2–methyl–1, 3–dioxolane; 2–methyl–1, 3–dioxolane–d4; 2–methyltetrahydrofuran; and methylcyclopentane, J. Raman Spectrosc. 1 (1) (1973) 17–45.
[45] M. Moskovits, K. Michaelian, A reinvestigation of the raman spectrum of water, J. Chem. Phys. 69 (6) (1978) 2306–2311.
[46] J.V. Castro, J.C. Cordeiro, F.J. Baceti, C.R. Blanco, G.V. Olivieri, R. Cella, N.H. Morgon, R.B. Torres, Molecular interactions between 2-methyltetrahydrofuran and alcohols: A combination of thermodynamic, spectroscopic and quantum chemistry studies, J. Mol. Liq. 394 (2024) 123755, http://dx.doi.org/10.1016/j.molliq.2023.123755.
[47] R. Bro, Multivariate calibration, Anal. Chim. Acta 500 (1-2) (2003) 185–194, http://dx.doi.org/10.1016/S0003-2670(03)00681-0.
[48] A. Wakisaka, S. Mochizuki, H. Kobara, Cluster formation of 1-butanol–water mixture leading to phase separation, J. Solution Chem. 33 (6/7) (2004) 721–732, http://dx.doi.org/10.1023/B:JOSL.0000043636.35477.89.
[49] F. Li, Z. Men, S. Li, S. Wang, Z. Li, C. Sun, Study of hydrogen bonding in ethanol-water binary solutions by raman spectroscopy, Spectrochimica acta. Part A, Molecular and biomolecular spectroscopy 189 (2018) 621–624, http://dx.doi.org/10.1016/j.saa.2017.08.077.
[50] M. Glass, M. Aigner, J. Viell, A. Jupke, A. Mitsos, Liquid-liquid equilibrium of 2-methyltetrahydrofuran/water over wide temperature range: Measurements and rigorous regression, Fluid Phase Equilib. 433 (2017) 212–225.
[51] S. Kumar, On phase inversion characteristics of stirred dispersions, Chem. Eng. Sci. 51 (5) (1996) 831–834, http://dx.doi.org/10.1016/0009-2509(96)90025-1.
[52] C. Reichardt, T. Welton, Solvents and Solvent Effects in Organic Chemistry, Wiley, 2010, http://dx.doi.org/10.1002/9783527632220.
[53] PEAXACT, S-PACT GmbH, Aachen, Germany, 2023.
[54] T. Fukasawa, Y. Tominaga, A. Wakisaka, Molecular association in binary mixtures of tert-butyl alcohol–water and tetrahydrofuran–heavy water studied by mass spectrometry of clusters from liquid droplets, J. Phys. Chem. A 108 (1) (2004) 59–63, http://dx.doi.org/10.1021/jp031011s.
[55] M. Katayama, K. Ozutsumi, The number of water-water hydrogen bonds in water-tetrahydrofuran and water-acetone binary mixtures determined by means of X-ray scattering, J. Solution Chem. 37 (6) (2008) 841–856, http://dx.doi.org/10.1007/s10953-008-9276-0.